Supporting Information

Yu et al. 10.1073/pnas.1117990109

SI Text

Topography of Terminated $La_{0.7}Sr_{0.3}MnO_3$ Thin Films. Atomic force microscopy (AFM) measurements were used to probe the nature of the surface of $La_{0.7}Sr_{0.3}MnO_3$ (LSMO) thin films with nominal $La_{0.7}Sr_{0.3}O$- and MnO_2-terminations following growth, as shown in Fig. S2. The morphology of both samples, which are grown via the layer-by-layer process, is very smooth and shows the presence of atomically flat terraces as defined by the underlying vicinal substrate and separated by steps of height approximately 0.4 nm (the lattice of one perovskite unit cell). Thus, the thin films grown in such a manner must be singly terminated. Combining this with the TOF-ISARS data, we are confident that the termination of the LSMO layer could be controlled by the growth.

Time-of-Flight Ion Scattering and Recoiled Ion Spectroscopy (TOF-ISARS). To confirm the termination control of the LSMO thin films, time-of-flight ion scattering and recoiled ion spectroscopy was used. This technique combines several ion spectroscopy techniques [ion scattering spectroscopy (ISS), direct recoil spectroscopy (DRS), and mass spectroscopy of recoiled ions (MSRI)], and is capable of highly sensitive surface composition analysis with isotope resolution. A schematic figure of the experimental setup is shown in Fig. S3*A*. During the experiments, low-energy (approximately 10 keV) pulsed potassium ions are injected onto the film surface at a grazing incident angle. As a consequence of the direct collision between the incoming ions and the surface, the elements at the topmost surface will be ionized. The created ion beam then travels through the acceleration zone with an applied electric field, with the final velocity of the ions depending on the mass-to-charge ratio. Finally, a constant electrostatic field is applied inside the reflection zone to bend the path of the ion beam toward the detector. Thus, by measuring the time needed for the ions to reach the detector, the mass-to-charge ratio of the ions is determined.

Due to the small penetration depth of the low-energy K ions, variable surface sensitivity is realized by choosing different incident angles for the ion beam. Fig. S3*B* presents the data measured with 15° incident angle. For comparison, the data were normalized at ^{55}Mn peak. Clearly, the LSMO film grown on thin SRO buffer layer exhibits enhanced intensities of La- and Sr-peaks. However, the difference between the two samples is relatively small compared with the results obtained with smaller incident angle (approximately 5°, Fig. 1*D*), which strongly supports the surface-sensitive nature of this method.

Layer Architecture of BFO/LSMO Heterostructures with Different Terminations. To confirm the atomic stacking sequence of the BFO/LSMO heterointerfaces, scanning transmission electron microscopy (STEM) was carried out to probe the local atomic structure of the samples. Fig. S4 *A* and *B* show the layer architectures of samples with both MnO_2- ($La_{0.7}Sr_{0.3}O$-MnO_2-BiO-FeO_2) and $La_{0.7}Sr_{0.3}O$- (MnO_2-$La_{0.7}Sr_{0.3}O$-FeO_2-BiO) terminated interface atomic stacking sequences, respectively. For both structures, the growth direction is from left to right. The MnO_2 terminated interface consists of a BFO/LSMO bilayer grown on the STO substrate (Fig. S4*A*). The LSMO layer is nominally 13 unit cells thick, and the BFO layer is approximately 21 nm thick. Similarly, the $La_{0.7}Sr_{0.3}O$ terminated interface consists of a heterostructure of SRO, LSMO, and BFO grown on the STO substrate (Fig. S4*B*), with a nominal layer thickness of 2.5 unit cells for SRO, 13 unit cells for LSMO, and approximately 27 nm for BFO. For both heterostructures, the cross-section STEM imaging suggests atomically abrupt and highly controlled epitaxial interfaces between the LSMO and the BFO layers.

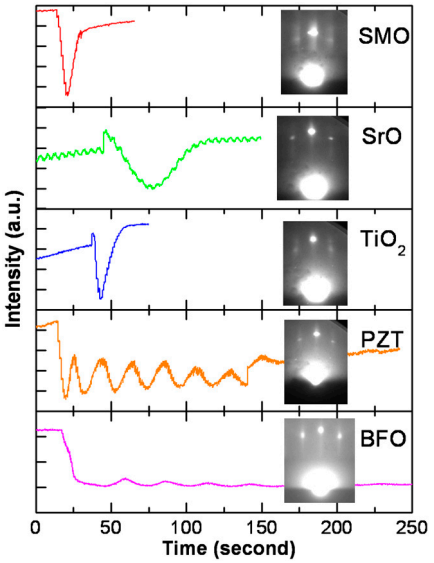

Fig. S1. Design of the heterointerface by epitaxial growth. RHEED pattern and the specular intensity monitored during the growth of various oxide materials. The clear intensity oscillations indicate the layer-by-layer growth mode for all the materials, which leads to the atomic-scale control of the heterointerface, therefore providing a solid platform for the current study.

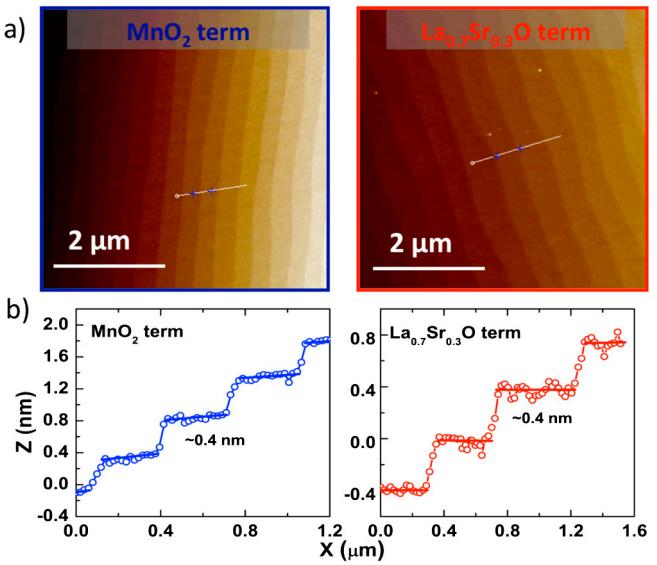

Fig. S2. Topography of LSMO thin films with nominal $La_{0.7}Sr_{0.3}O$ and MnO_2 terminations. (*A*) Atomic force microscopy images of films terminated by MnO_2 (*Left*) and $La_{0.7}Sr_{0.3}O$ (*Right*). (*B*) Line scans across the AFM images showing atomically flat terraces with a step height of approximately 0.4 nm (the lattice constant of one perovskite unit cell).

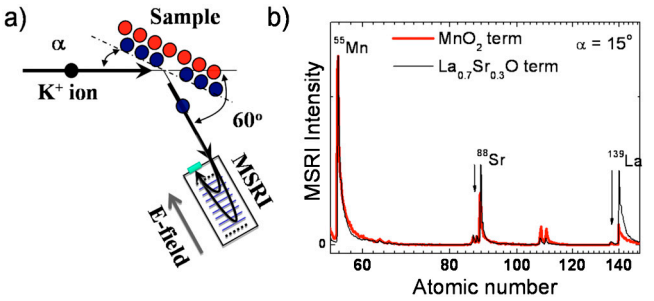

Fig. S3. TOF-ISARS spectra of MnO_2- and $La_{0.7}Sr_{0.3}O$-terminated $La_{0.7}Sr_{0.3}MnO_3$ thin films. (*A*) Schematic of the TOF-ISARS experiment setup. (*B*) MSRI spectra of LSMO thin films with nominal MnO_2 and $La_{0.7}Sr_{0.3}O$ terminations measured with an incident angle of 15°. Different surface sensitivity can be realized in the measurement by changing the incident angle of the ion beam.

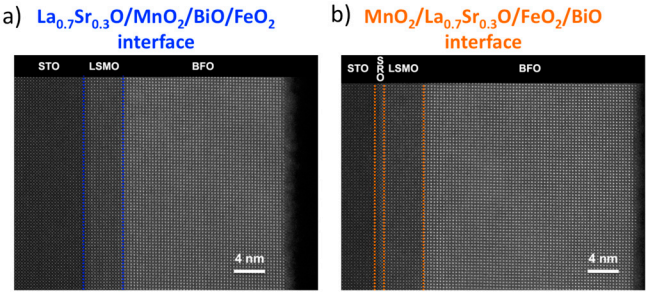

Fig. S4. Layer architecture of BFO/LSMO with different terminations measured with scanning transmission electron microscopy. (*A*) The sample with the MnO_2-terminated ($La_{0.7}Sr_{0.3}O$-MnO_2-BiO-FeO_2) interface is designed by growing integral unit cells LSMO layer directly on STO substrates, followed with the growth of the BFO layer. (*B*) For the sample with the $La_{0.7}Sr_{0.3}O$-terminated (MnO_2-$La_{0.7}Sr_{0.3}O$-FeO_2-BiO) interface, 2.5 unit cells of $SrRuO_3$ are deposited on STO to switch the termination of the STO from TiO_2 to SrO. Images obtained with the TEAM 0.5 microscope at NCEM.

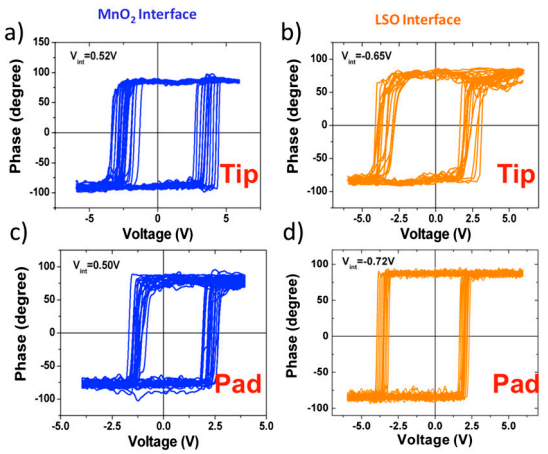

Fig. S5. Comparison of biased-voltages for BFO heterostructure with both MnO_2- (*A* and *C*) and $La_{0.7}Sr_{0.3}O$- (*B* and *D*) terminated interfaces measured with PFM tips (*A* and *B*) and Au electrodes (30 μm squares with a thickness of 100 nm) (*C* and *D*) as top contacts. Both methods reveal the presence of a consistent biased-voltage in their respective loops, which are correlated with the interface atomic stacking sequences. The measured biased-voltages differences between different interface terminations through both methods are almost identical: with 1.17 V (0.52 V + 0.65 V) for PFM tips and 1.22 (0.50 V + 0.72 V) for Au electrodes.

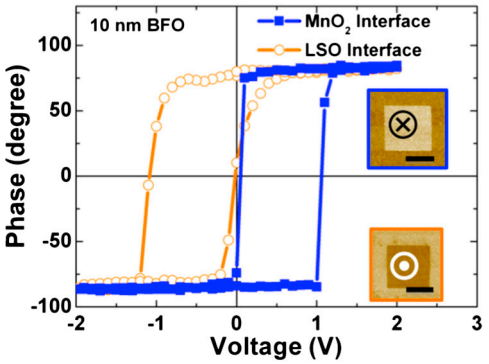

Fig. S6. Typical piezoresponse hysteresis loops for 10 nm BFO samples with both MnO_2 (blue) and $La_{0.7}Sr_{0.3}O$ (yellow) interfaces. *Insets* show the out-of-plane PFM images of 10 nm BFO samples with MnO_2- (*Top*) and $La_{0.7}Sr_{0.3}O$- (*Bottom*) terminated LSMO bottom electrodes. The length of scale bars is 2 μm for both images.

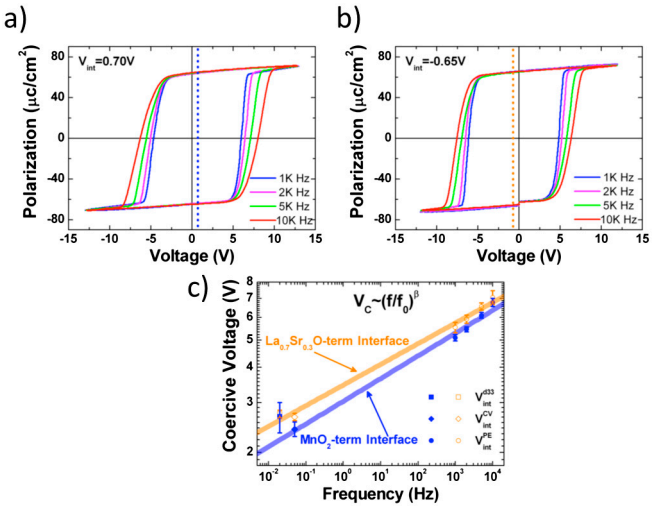

Fig. S7. Ferroelectric hysteresis loops for BFO thin films (150 nm) with both MnO_2 (*A*) and LSO (*B*) interface configurations. (*C*) Summary of frequency dependent coercive fields for both interface configurations.

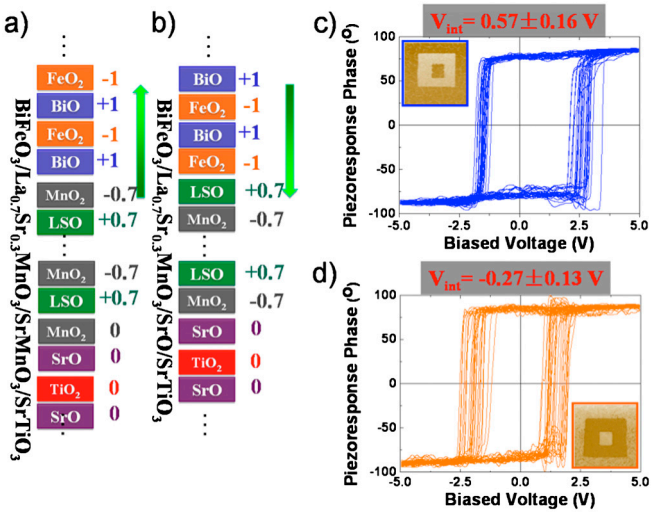

Fig. S8. Alternative pathways to engineer two possible STO/LSMO interface terminations in the STO/LSMO/BFO heterostructures and the corresponding piezoelectric hysteresis loops. (*A*) Schematic diagram of the atomic stacking sequence for the heterostructure with SrO-MnO_2 (STO/LSMO) and MnO_2-BiO (LSMO/BFO) interfaces and the corresponding ferroelectric hysteresis loop (*C*). (*B*) Schematic diagram of the atomic stacking sequence of the heterostructure with SrO-MnO_2 (STO/LSMO) and $La_{0.7}Sr_{0.3}O$-FeO_2 (LSMO/BFO) interfaces and the corresponding ferroelectric hysteresis loop (*D*). *Insets* of *C* and *D* show the out-of-plane PFM images of the corresponding structures. The structure shown in *A* is fabricated with the growth sequence of 75 nm BFO/12 unit cells LSMO/1 unit cell of $SrMnO_3$ on the STO substrate. Similarly, the one shown in *B* is designed with the growth sequence of 75 nm BFO/13 unit cells LSMO/one monolayer of SrO on STO substrate. For both samples, despite the fact that they bear identical LSMO/STO interface structures, the ferroelectric polarization electronic reconstructions are exactly opposite. This highlights the deterministic role of the LSMO/BFO interface on the current ferroelectric polarization control.

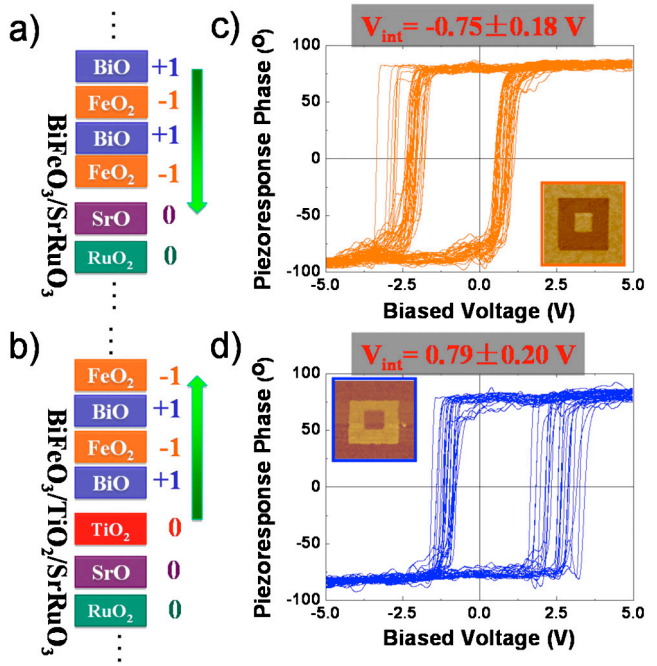

Fig. S9. Schematic diagram of the atomic stacking sequence of the BFO/SRO heterostructure with RuO_2-SrO-FeO_2-BiO (*A*) and RuO_2-SrO-TiO_2-BiO-FeO_2 (*B*) interfaces, and the corresponding local piezoelectric hysteresis measurements (*C* and *D*). PFM measurements are shown in *Insets* (*C* and *D*). During the epitaxial growth, the SRO layer will be self-terminated with SrO because Ru is volatile at the growth temperature. Thus, the RuO_2-SrO-FeO_2-BiO interface is designed by growing BFO directly on SRO/STO. The RuO_2-SrO-TiO_2-BiO-FeO_2 interface was achieved by inserting one monolayer of TiO_2 between BFO and SRO.

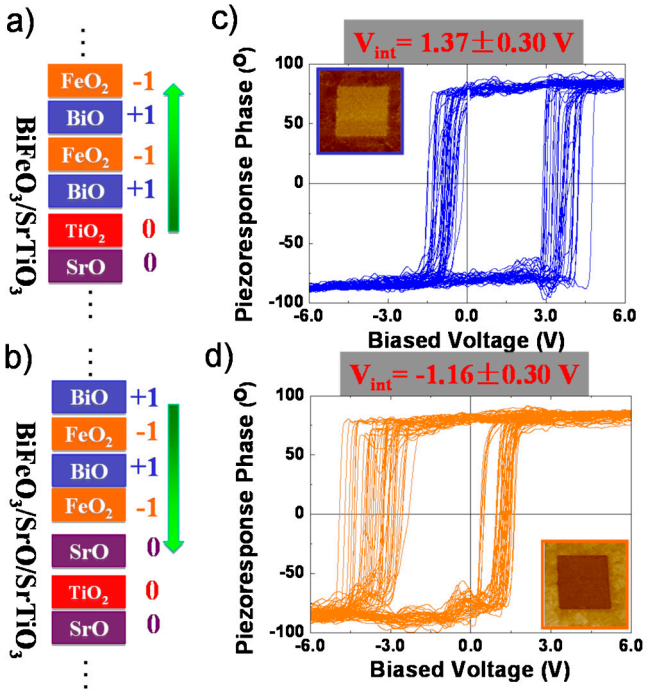

Fig. S10. Schematic diagram of the atomic stacking sequence of BFO/STO heterostructure with SrO-TiO_2-BiO-FeO_2 (*A*) and TiO_2-SrO-FeO_2-BiO (*B*) interfaces, and the corresponding local piezoelectric hysteresis measurements (*C* and *D*). PFM measurements are shown in *Insets* (*C* and *D*). The SrO-TiO_2-BiO-FeO_2 interface is designed by growing BFO directly on TiO_2-terminated STO. The TiO_2-SrO-FeO_2-BiO interface was achieved by inserting one monolayer of SrO between BFO and STO.

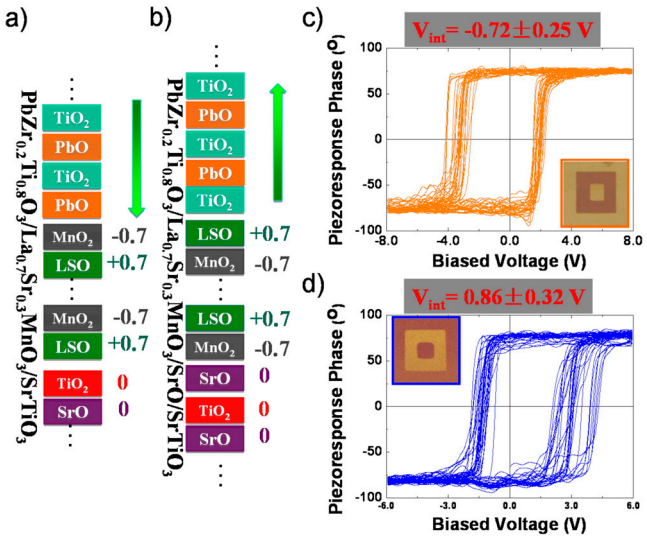

Fig. S11. Schematic diagram of the atomic stacking sequence of the PZT/LSMO heterostructure with $La_{0.7}Sr_{0.3}O$-MnO_2-PbO-$Zr_{0.2}Ti_{0.8}O_2$ (*A*) and MnO_2-$La_{0.7}Sr_{0.3}O$-$Zr_{0.2}Ti_{0.8}O_2$-PbO (*B*) interfaces, and the corresponding local piezoelectric hysteresis measurements (*C* and *D*). PFM measurements are shown in *Insets* (*C* and *D*).